Ji et al.
Chinese Journal of Mechanical Engineering (2023) 36:46
https://doi.org/10.1186/s10033-023-00877-7

Chinese Journal of Mechanical Engineering

ORIGINAL ARTICLE

Open Access

Microstructure, Properties and Crack Suppression Mechanism of High-speed Steel Fabricated by Selective Laser Melting at Different Process Parameters

Wenbin Ji[1,2*], Chuncheng Liu[1,2], Shijie Dai[1,2] and Riqing Deng[1,2]

Abstract

To enrich material types applied to additive manufacturing and enlarge application scope of additive manufacturing in conformal cooling tools, M2 high-speed steel specimens were fabricated by selective laser melting (SLM). Effects of SLM parameters on the microstructure and mechanical properties of M2 high-speed steel were investigated. The results showed that substrate temperature and energy density had significant influence on the densification process of materials and defects control. Models to evaluate the effect of substrate temperature and energy density on hardness were studied. The optimized process parameters, laser power, scan speed, scan distance, and substrate temperature, for fabricated M2 are 220 W, 960 mm/s, 0.06 mm, and 200 ℃, respectively. Based on this, the hardness and tensile strength reached 60 HRC and 1000 MPa, respectively. Interlaminar crack formation and suppression mechanism and the relationship between temperature gradient and thermal stress were illustrated. The inhibition effect of substrate temperature on the cracks generated by residual stresses was also explained. AM showed great application potential in the field of special conformal cooling cutting tool preparation.

Keywords Selective laser melting, High-speed steel, Mechanical properties, Microstructure, Interlaminar cracks

1 Introduction

Additive manufacturing (AM) technology is a new manufacturing technology, unlike traditional manufacturing technology. The AM technology, which is directly informed by 3D model data, is being rapidly developed as a potential production method in several industries [1]. AM technology has many significant characteristics such as delivering intricate, complex geometries and short lead times [1]. It is widely used in aerospace [2], biomedical [3], construction, and many other fields [4–6]. Selective laser melting (SLM) is one of the main methods for AM. Metal components produced via SLM technology offer equivalent or sometimes superior mechanical properties to those of bulk materials [7].

The materials suitable for AM technology are not only limited to engineering plastics such as ABS resin, polylactic acid (PLA), and polyamide (PA) [8], but also equally apply to metals such as stainless steel [7], tool steel, pure copper, nickel-chromium base superalloy [9], and titanium alloy [4]. With the continuous increase in market demand, the direction of manufacturing functional parts is changing. Therefore, the research on metals has not been interrupted. However, the application in AM of metal tool materials is less. M2 high-speed steel (HSS) is one of the earliest HSS materials widely available in the world. To overcome the defects of coarse carbides,

*Correspondence:
Wenbin Ji
2017082@hebut.edu.cn
[1] State Key Laboratory of Reliability and Intelligence of Electrical Equipment, Hebei University of Technology, Tianjin 300130, China
[2] School of Mechanical Engineering, Hebei University of Technology, Tianjin 300130, China

severe segregation, high contents of reticular carbides and nonmetallic inclusions that are easily generated by the conventional melting method in fabricating HSS, AM technology provides a new forming method. Moreover, additively manufactured inserts or drills with integrated cooling channels have the potential to increase productivity enormously [6].

Khorasani et al. [10] studied the performance of SLM-formed parts under different process parameters. A high laser power and low scanning speed can transfer energy preferably and produce a good quality molten pool, which can increase the hardness of materials. In addition, when the laser scanning distance is lower than the optimal laser scanning distance, the hardness decreases due to a large overlap. When the laser scanning distance is higher than the optimal laser scanning spacing, the hardness decreases due to the dispersion of laser beam energy. Liverani et al. [7] introduced the microstructure and mechanical properties of the AISI316L sample prepared by the SLM method, and the experimental results showed that laser power has the strongest influence on density. The highest relative density was obtained at the highest investigated power level (150 W), while hatch spacing and building orientation do not significantly affect the tested range. Nguyen et al. [11] optimized the process parameters such as the laser power, scanning speed, laser spot diameter, and scanning distance, thus forming a nearly full dense 304L stainless steel sample. Sun et al. [12] analyzed the macroscopic and microscopic structure of SLM molded titanium alloy parts; when the laser power was higher than 175 W, the sensitivity of density to laser energy decreased with the increase in laser power and the decrease in scanning speed.

Metal AM can overcome the limitations of traditional design and manufacturing, achieving a lighter weight, excellent performance, and high efficiency for the components fabricated. However, the complex selective melting of laser leads to many defects in the forming of metal parts. During fabrication, metallic AM parts/alloys experience a complex thermal history involving directional heat extraction and repeated melting and rapid solidification. Many alloys also experience repeated solid-state phase transformations. These factors introduce complexities to the analysis of microstructural evolution and properties not typically found in conventional processes [13]. Yakout et al. showed the existence of an optimal energy density in SLM. When it is lower than this value, spherical defects will lead to the void formation, and when it is higher than this value, vaporization will occur [14]. Rapid melting and solidification during SLM manufacturing lead to a higher cooling rate and temperature gradient in the molten pool [15]. Therefore, SLM is inevitably accompanied by high residual stress levels [4]. Typical SLM defects also include cracking, substrate adherence and warping, and swelling [16]. The formation of defects is essentially dependent on the process variables, which should be optimized to fabricate defect-free components [17]. For the SLM forming difficulty of M2 high-speed steel, the combination of brittle and rigid materials with the SLM forming process results in high residual stress, which is easy to form interlayer cracks or parts and substrate delamination, which greatly limits the application of high-speed steel materials. At present, the most effective way to solve this problem is to reduce the thermal stress by increasing the substrate temperature to reduce the temperature gradient, so as to reduce the number of cracks between layers.

In this paper, HSS was used as the experimental material. The optimal process parameters of SLM in the formation of M2 HSS such as laser power, scan speed, scan distance, and substrate temperature were evaluated. M2 HSS samples were prepared with different process parameters by performing Taguchi experiments. Then, the effect of process parameters on the hardness, tensile strength, phase composition, and microstructure was analyzed. The results provide an experimental basis for the formation of a conformal cooling M2 high-speed steel end milling cutter using SLM.

2 Experimental Procedures

2.1 Raw Materials and Equipment

$W_6Mo_5Cr_4V_2$ powder was prepared using a gas atomization method. Chemical components of the HSS ($W_6Mo_5Cr_4V_2$) powder are shown in Table 1.

The morphology of $W_6Mo_5Cr_4V_2$ HSS powder is shown in Figure 1. The powder has the characteristics of high sphericity, low oxygen content, uniform particle size distribution, good fluidity, and high bulk density and tap density. The original product was sieved with a 200 mesh sieve to remove the coarse powder which affects printing. The particle size distribution is 15–53 μm, where $D_{V10} = 22.3$ μm, $D_{V50} = 34.8$ μm, and $D_{V90} =$

Table 1 Chemical composition of the HSS ($W_6Mo_5Cr_4V_2$) powder

Chemical composition(wt %)								
Elements	**W**	**Mo**	**Cr**	**V**	**C**	**Si**	**Mn**	**Fe**
wt %	5.53	4.51	3.86	1.83	0.827	0.38	0.27	Bal.

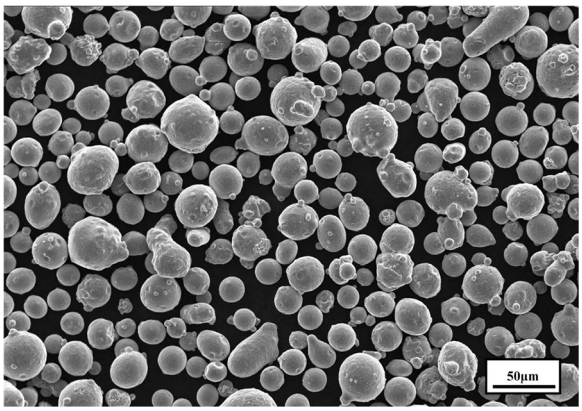

Figure 1 The morphology of $W_6Mo_5Cr_4V_2$ HSS powder

54.4 μm. The particle size conforms to normal distribution. The powder oxygen content is 0.0339 wt%, and the nitrogen content is 0.0590 wt%.

An IGAM-I metal printer with a maximum power of 500 W, laser wavelength of 1070 nm, a laser spot diameter of 0.1 mm, and a focal length of 128 μm from Yibo 3D Technology Company (China) was used in this work. The maximum forming size of the experimental equipment is 103 mm × 103 mm × 200 mm. The forming principle diagram and process of the metal powder molding machine in the experiment are shown in Figures 2 and 3.

2.2 Experimental Design

Because the physical properties of M2 HSS and 316L stainless steel are similar, a comparison of the physical properties of HSS and stainless steel is shown in Table 2. Therefore, the SLM process parameters of M2 HSS were determined according to those of 316L stainless steel. It is possible to obtain near-full density samples with ultimate tensile strength and elongation to failure higher than those obtained with conventionally processed AISI316L [7]. The preliminary experimental results indicate that the specimens were broken or exhibited only a low strength due to the trouble of cracks no matter how the parameters were adjusted while studying the interaction between laser power, scan speed, scan distance, and layer thickness. Hereby, under a layer thickness of 30 μm, the substrate temperature was introduced to reduce the temperature gradient. Moreover, the coupled mechanism among the laser power, scan speed, scan distance, and substrate temperature was studied in-depth. According to previous studies [18], the high density parts were produced with a scan speed of above 700 mm/s to achieve a uniform microstructure and hardness. Therefore, more than 700 mm/s scan speeds were selected to explore the best parameters.

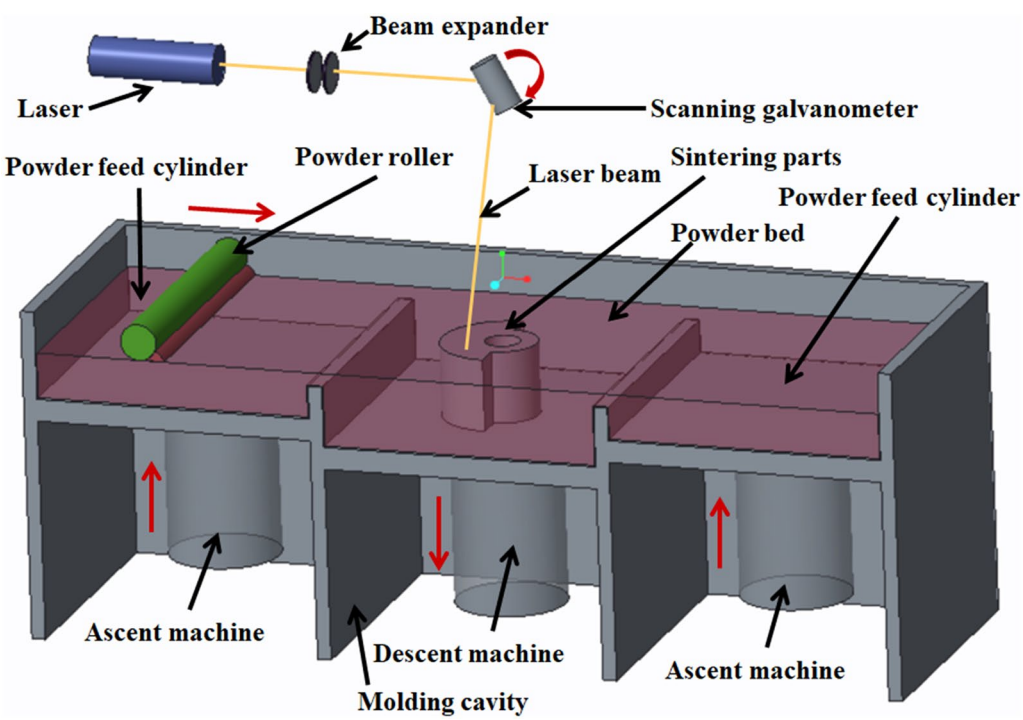

Figure 2 Forming principle diagram

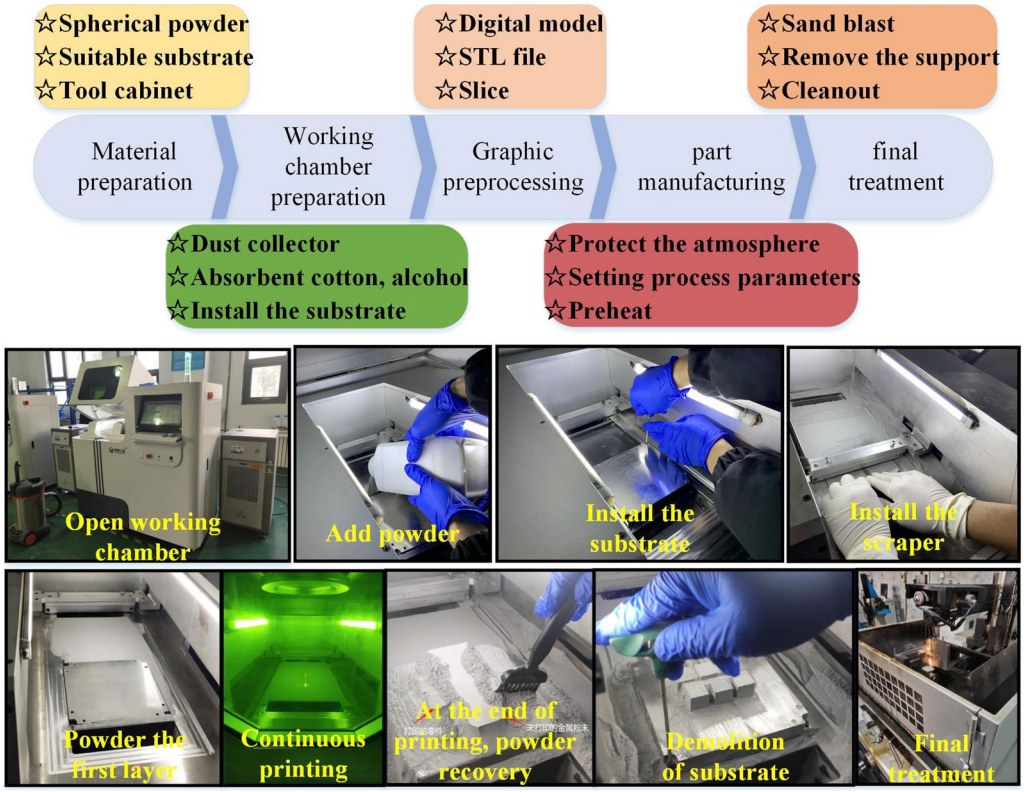

Figure 3 Metal printing process in laser selective melting

Table 2 Comparison of the physical properties between HSS and stainless steel

Physical Properties	Physical properties	Physical properties
Density(g/cm^3)	8.14	7.9
Melting point(℃)	1520	1400
Elastic modulus(GPa)	210	198
Heat resistance(℃)	500–600	300–400
Hardness	62–64 HRC	230 HV
thermal expansivity(℃)	11×10^{-6}	17.3×10^{-6}
Bending strength(GPa)	2.5–4	2.4
Compressive strength(GPa)	2.8–3.8	4
Thermal conductivity(W/(m·K))	19.0	16.2

Due to there being few references for SLM forming of M2 high-speed steel, and existing studies only showing that the substrate temperature has an effect on SLM forming high-speed steel, there is no guidance for SLM forming M2 high-speed steel based on the comprehensive effect of various process parameters. Therefore, through exploration and a large number of experimental verification in the early stage, we finally determined to optimize the process parameters by an orthogonal experiment of four factors. The laser power, scan speed, scan distance, and substrate temperature were selected as variable factors. The rest parameters were constant, such as a laser spot diameter of 0.1 mm, 90° rotation angle of each layer, layer thickness of 30 μm, and scanning once per layer. The Taguchi experimental factors and levels for SLM forming M2 HSS are shown in Table 3.

Table 3 Factors and levels of Taguchi experimental

Factors Levels	Laser power *P*(W)	Scan speed *v*(mm/s)	Scan distance *h*(mm)	Substrate temperature *T*(℃)
1	180	870	0.06	50
2	200	960	0.07	100
3	220	1050	0.08	150
4	240	1140	0.09	200

2.3 Text Methods

2.3.1 Hardness and Tensile Tests

The tensile and cubic specimens were formed directly on the 316L stainless steel substrate according to the size requirements. The specimens were then separated from the substrate by wire cutting. Before testing

the hardness, the samples were ground with 400, 600, 800, and 1200 mesh sandpaper. All the samples were polished using a P-1 polishing machine after grinding. Then, a surface roughness measuring instrument (TIME 3200 stylus, China) was used to ensure that the surface roughness of the samples was less than 0.1 μm. The hardness of SLM samples was measured using a Rockwell hardness tester (Grows HRS-150, China) under a force of 150 kg for 10 s dwell time, and each specimen was estimated from the average value of five measured points. All the sample surfaces were ground with sandpaper and filed to prevent the presence of small defects affecting the tensile strength. After grinding, the width and thickness of each sample were measured, and the tensile properties were evaluated using an E 10000 electronic dynamic and static fatigue tester. The tensile strengths were obtained from each group of parameters. Five tensile samples were printed for each process parameter, and the average value was taken as the strength of the corresponding process parameter. The size of the specimens is shown in Figure 4.

2.3.2 Microstructural Characterization

The SLM-processed samples were subjected to X-ray diffraction (XRD) analysis (SmartLab 9, Japan) to detect the phases within the 2θ range of 5°–80°. The macrostructure and microstructure of the samples were observed using an optical microscope (ZEISS Smartzoom 5, Germany) and S-4800 field-emission SEM. Before observation, the samples were ground, polished, and corroded with a mixture of diluted 10% hydrofluoric acid, nitric acid, and alcohol. Corrosion should be appropriate. Over-corrosion shows a false phase of improved inhomogeneity with blackened carbide.

3 Results and Discussion

3.1 Mechanical Properties

3.1.1 Hardness

The hardness and tensile performance of M2 HSS prepared under different SLM processes are shown in Table 4. Most of the hardness was concentrated in the 55–60 HRC, except a minority of that in the 50–55 HRC. The hardness of only two groups was lower than 50 HRC, which were 42.03 HRC and 43.40 HRC. The variance analysis of various factors showed that hardness is mainly affected by the scan distance. According to the results of range analysis, the effect of various factors on the hardness of SLM M2 HSS decreases in the order of scan distance > substrate temperature > laser power > scan speed. The optimal combination is laser power 220 W, scan speed 960 mm/s, scan distance 0.06 μm, and substrate temperature 200 °C.

A qualitative comparison of various factors affecting the hardness of specimens is shown in Figure 5. Scan distance is the main factor affecting hardness. The main reason is when the scan distance mildly changes from 0.08 mm to 0.09 mm, the hardness sharply decreased. The metal powder changes into a liquid status when illuminated by the laser beam, and a large spacing will make it harder to overlap between adjacent scanning trajectories. It leads to a severe decrease in density and hardness. A large scan distance leads to the failure of powder at a scan trajectory of sample surface to form effective bonding, causing the appearance of determinant holes on the sample surface. Figure 6 shows the surface morphology when the scan distance was 0.09 mm. The scan distance slightly affected the hardness when it was decreased from 0.08 mm to 0.07 mm by only 0.85 HRC. The effects of laser power, scan speed, and substrate temperature on the hardness were 4.56 HRC, 3.37 HRC, and 5.11 HRC, respectively. Therefore, it is necessary to reduce the scan distance to a certain value and ensure that the

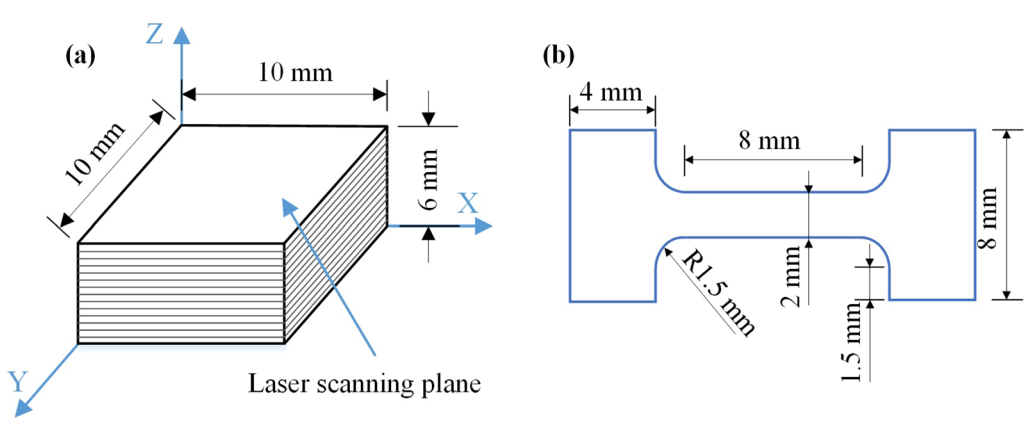

Figure 4 Cubic specimen formed by SLM and size of tensile specimen **a** Cubic specimen, **b** Tensile specimen

Table 4 The hardness and tensile properties of M2 HSS prepared under different SLM processes

NO.	The level of each factor				*H* (HRC)	*σ* (MPa)	*E* (J/mm^3)
	P	*v*	*h*	*T*			
1	180	870	0.06	50	54.20	219.49	114.94
2	180	960	0.07	100	50.27	506.58	89.29
3	180	1050	0.08	150	50.93	714.97	71.43
4	180	1140	0.09	200	49.83	607.93	58.48
5	200	870	0.07	150	57.23	185.38	109.47
6	200	960	0.06	200	58.53	936.92	115.74
7	200	1050	0.09	50	42.03	253.46	70.55
8	200	1140	0.08	100	51.05	719.75	73.10
9	220	870	0.08	200	58.97	782.34	105.36
10	220	960	0.09	150	56.85	619.75	84.88
11	220	1050	0.06	100	56.83	716.78	116.40
12	220	1140	0.07	50	54.43	150.87	91.90
13	240	870	0.09	100	43.40	214.43	102.17
14	240	960	0.08	50	56.77	246.15	104.17
15	240	1050	0.07	200	59.17	705.02	108.84
16	240	1140	0.06	150	57. 00	549.55	116.96

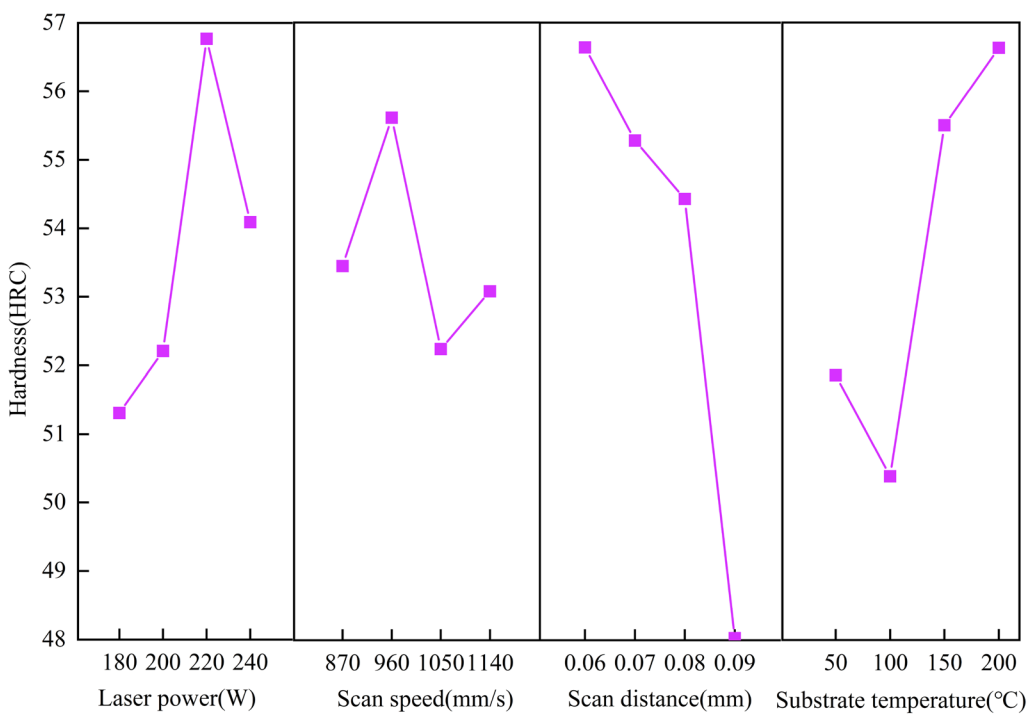

Figure 5 Taguchi experimental curve on hardness

laser power, scan speed, and substrate temperature have a feeble influence on the hardness reduction, ensuring that the hardness of the sample reaches a higher level. Moreover, the hardness values always maintained a relatively high level when the scan distance was in the range of 0.06–0.08 mm. The effect of scanning distance on hardness can be attributed to the fact that the sample cannot be densified due to a too large scanning distance.

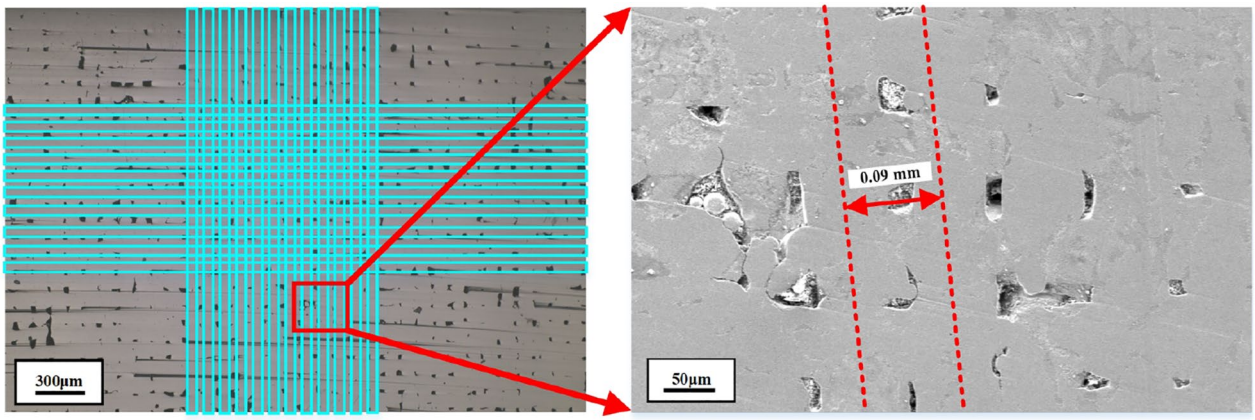

Figure 6 The surface morphology at the scan distance of 0.09 mm

Therefore, it is considered that the substrate temperature has the greatest impact on the experiment and is more valuable for research when the scan distance is within a suitable range.

The effect of substrate temperature on hardness shows a trend of first decreasing and then increasing with the increase in substrate temperature, and the hardness increases sharply in the range of 100–150 °C. The rapid cooling of the molten pool inhibits the growth of grains and the segregation of alloy elements, making the solid-soluble alloy elements in the metal matrix unable to precipitate and uniformly distribute in the matrix. Therefore, a microstructure with fine grains and uniform microstructure was obtained in SLM forming, i.e., with the increase in substrate temperature, the grain size increases, and the hardness decreases. This indicates that grain strengthening does not play a leading role in the strengthening mechanism. The content of ferrite and martensite in the sample with a high substrate temperature increased, indicating that the increase in substrate temperature contributed to the increase in austenite content before martensite transformation. The higher the carbon content of austenite, the greater the saturation of martensite, and the higher the hardness. The effect of substrate temperature on the hardness did not exhibit a downward trend when the maximum temperature in the experiment was 200 °C. To further improve the hardness, subsequent studies can continue to improve the substrate temperature to evaluate the effect of the inflection point of substrate temperature on hardness. Figure 7 shows a high hardness with high energy density and high substrate temperature. Subsequent research can continue to explore the superior performance of HSS in these two directions.

The hardness increases with the increase in laser power from 180 to 220 W, and radically changes in the range of

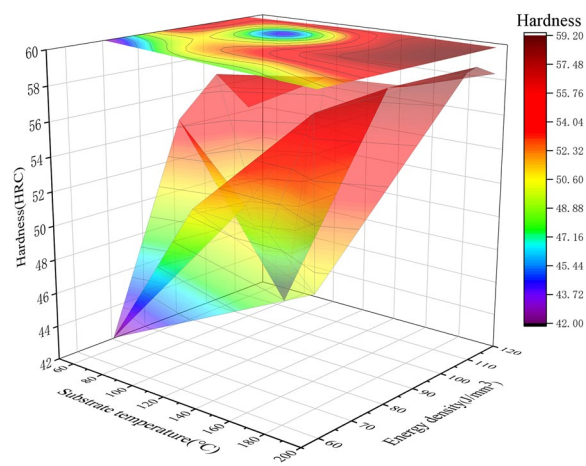

Figure 7 Effect of energy density and substrate temperature on hardness

200–220 W. According to the energy density equation ($E=P/(v\cdot h\cdot L)$, $L=30$ μm), the energy density is directly proportional to the applied laser power. Therefore, the lack of laser beam energy during the preparation of sample will cause the incomplete fusion of metal powder, which cannot achieve effective bonding between the liquid phase and form undesired pores, as shown in Figure 8(a). When the laser power is enough to completely melt the metal powder of HSS, the liquid flow between each layer increases. Consequently, the number of pores on the sample gradually decreases, and the density and hardness increase. However, the laser power increases to a certain extent (220–240 W), and the hardness of sample decreases. Although the probability of porosity decreases with the increase in laser power, due to higher thermal stress and the relative instability of liquid phase when the energy density is too high, fine micro-cracks and balling occurred, as shown in Figure 8(b) and (c), thus

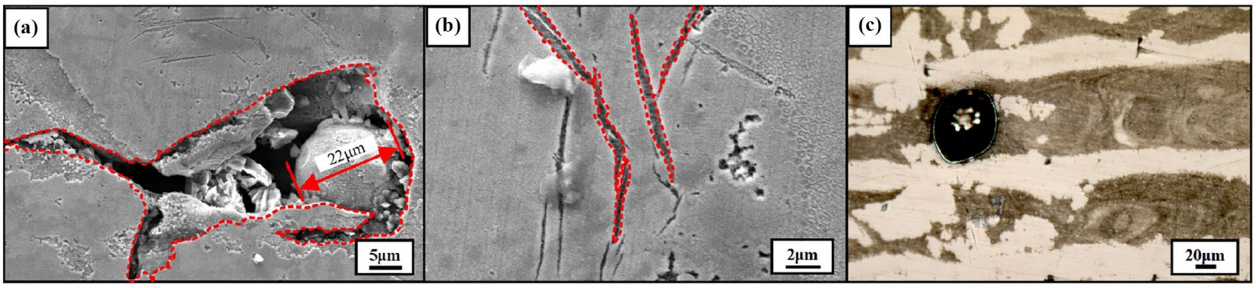

Figure 8 Typical forming defects **a** irregularly shaped pores due to insufficient melting; **b** and **c** micro-cracks and balling in SLM HSS sample due to over-high laser power

resulting in a decrease in hardness. The condensation of molten liquid metal under the action of surface tension will result in balling. The formation of balling not only reduces the tensile strength and fatigue resistance of the component, but also affects the quality of the next layer of powder, resulting in the accumulation of defects and affecting the quality of the whole component.

The effect of scan speed on hardness is nonsignificant. The hardness first increases and then decreases significantly and then increases with the increase in scanning speed. When the scan speed was at a relatively low level, the energy density was large, and the samples showed warping, cracks, and other defects, affecting the surface quality. With the increase in scanning speed, the liquid phase can be fully spread within the metal layers in an appropriate range, so the hardness is improved. However, the decreased energy density was insufficient to completely melt the powder as the scan speed continued to increase, resulting in the transformation of the formed sample into many holes. The energy density significantly decreases due to too fast scan speed. At a low energy density, the hardness values were at a small level.

3.1.2 Tensile Strength

The tensile strength in mechanical properties is a very important index for evaluating the performance of materials. The ultimate aim for the development of any engineering material is to achieve superior properties, especially mechanical properties [19]. As shown in Table 4, the maximum tensile strength was 936.92 MPa. The variance analysis showed that the substrate temperature is the main factor affecting the strength. According to the results of range analysis, the effects of various factors on the strength of SLM M2 HSS decrease in the order of substrate temperature > scan speed > scan distance > laser power. The optimal combination was laser power 220 W, scan speed 1050 mm/s, scan distance 0.08 μm, and substrate temperature 200 °C.

The trend is shown in Figure 9. The tensile strength significantly improved with the increase in substrate temperature, because the cracks on the sample were eliminated. A large amount of thermal stress is produced during the transformation of austenite into martensite when the substrate temperature is low. When the thermal stress exceeds the fracture strength of the material, the material releases the thermal stress by cracking, i.e., the existence of large thermal stress leads to cracks in the sample. Cracks ruined the workpiece. The temperature gradient decreases with the increase in substrate temperature. Although the printed sample still generates thermal stress, it is insufficient to cause the sample to crack. Therefore, the tensile strength gradually increases. Future research can continue to increase the substrate temperature to evaluate the effect on the tensile strength of printed HSS in the printing equipment. Moreover, the residual stress in the sample can be removed by thermal aging or vibration aging, and then the tensile strength can be further improved. Both the laser power and scanning speed first increase and then decrease with intensity. A high laser power and low scan speed lead to an increase in energy density, leading to the over-sintering and warpage of the sample surface. At a low laser power or high scan speed, defects such as pores appear in the printed sample, which is unfavorable to the sample itself. The strength first decreases, then increases, and then decreases with the increase in scanning distance. The density of printed sample was superior due to the small scan distance (0.06 mm), resulting in high strength. The generated pores can release the internal residual stress and increase the strength again when the distance is 0.08 mm. The pores severely affected the inherent performance of the sample. The incomplete connection between the adjacent two melting channels during the scanning resulted in a decrease in strength when the scan distance was 0.09 mm.

Based on the above analysis of mechanical properties, it can be concluded that both the hardness and strength

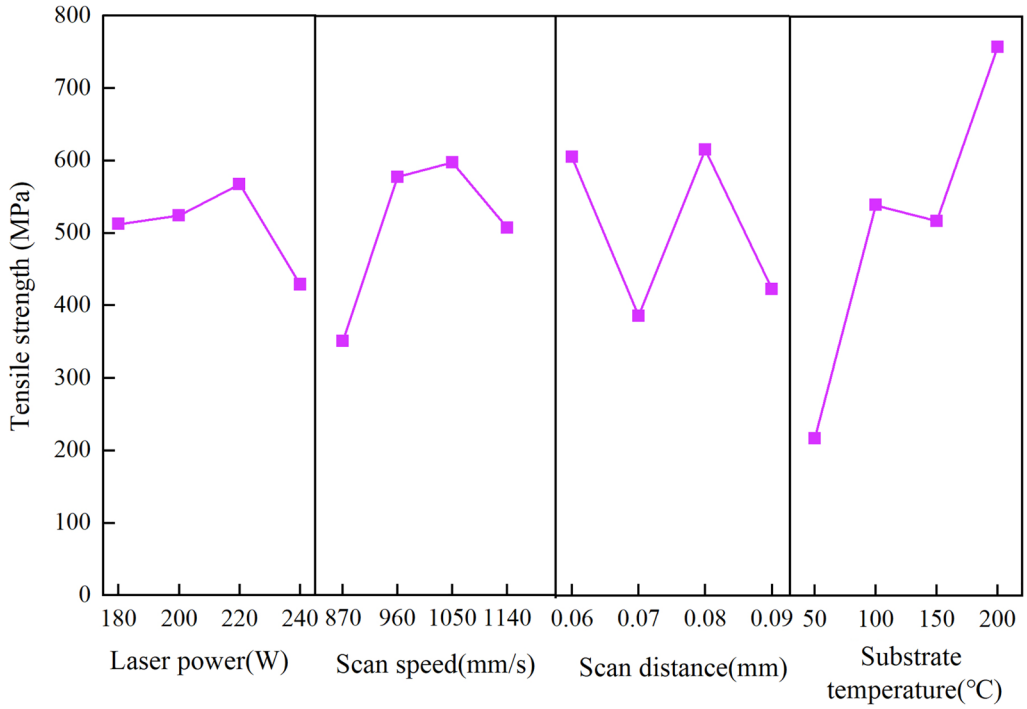

Figure 9 Taguchi experimental curve on strength

are at a high level with the optimized parameters. The laser power was 220 W, and the substrate temperature was 200 °C. The best parameters of scanning speed were 960 mm/s for hardness and 1050 mm/s for tensile strength. The tensile strength at a scan speed of 960 mm/s was basically the same as that at a scan speed of 1050 mm/s, but the hardness significantly decreases at a scan speed of 1050 mm/s. Therefore, the optimal scan speed parameter was 960 mm/s. Similarly, the scan distance was 0.06 mm.

3.2 Microstructure

3.2.1 Phase Composition

The XRD patterns of HSS samples at different substrate temperatures are shown in Figure 10. According to the annotation in the figure, the main phases are α-Fe, austenite, martensite, and MC carbides. After molding at different substrate temperatures, although the phase content is different, the diffraction peak intensity changes slightly. This indicates that the substrate temperature slightly affects the phase of SLM formed M2 HSS, and the formed sample transforms from austenite to martensite. The increase in cooling rate is beneficial for reducing the initial transformation temperature from austenite to martensite. However, no significant difference was observed in the phase content by changing the substrate temperature. Therefore, it can be considered that an increase in the substrate temperature can improve the printing quality when it can overcome the severe defects in the forming process. This has no severe influence on the phase composition, and the high energy density can be selected to achieve better results when the substrate temperature is increased.

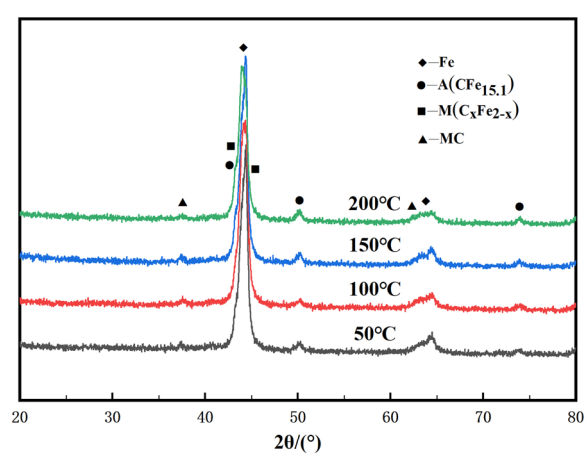

Figure 10 XRD patterns of HSS samples at different substrate temperatures

3.2.2 Surface Contour

The samples under different process parameters were ground and polished. The corrosive surface morphology of HSS was observed under an S-4800 electron microscope. The scanning rotation angle of each layer in the SLM process was 90°, as shown in Figure 11(a) The vertically staggered structure significantly improves the strength of the parts. The results show that the interlayer rotation angle slightly affects the parts, but the appropriate parameters of each layer rotation angle can be studied in the future.

Figure 11(b) shows the carbide with a network structure on the surface. According to the XRD analysis, MC carbides are present in the samples, mainly VC carbides. Moreover, a large number of columnar crystals are present. Because of the existence of such carbides and columnar crystals, the plastic deformation ability of the specimen decreases. The experimental results show that under the same energy density, the temperature gradient between the sample and substrate decreases, and the grain size increases with the increase in substrate temperature. The initial eutectoid carbides precipitate along the austenite grain boundary, which adversely affects the hardness and toughness of the steel when the cooling rate is slow. Because carbide precipitation reduces the supersaturation of carbon and alloy elements in the matrix, the hardening effect was weakened. The grain boundaries are weakened, resulting in the reduced toughness of steel in the carbide precipitate along the grain boundaries. Therefore, in the case that an increase in substrate temperature can improve the crack of parts, higher energy density helps to improve the cooling rate and significantly improves the toughness. In addition, inclusions, carbides, and the interface between carbides and matrix easily produced microcracks on HSS. Alloy carbide in HSS was hard and brittle, easily producing microcracks as shown in Figure 11(c). The irregular large size M2C and MC were prone to cracks in the HSS and became the source of cracks.

3.3 Interlaminar Cracks Suppression Mechanism

3.3.1 Characterization of Interlaminar Cracks

A high substrate temperature plays an important role in crack suppression during the SLM forming of M2 HSS. The side crack of cube specimens with a gradient of 50 °C appeared from (a) to (d) when the substrate temperature was in the range of 50–200 °C, as

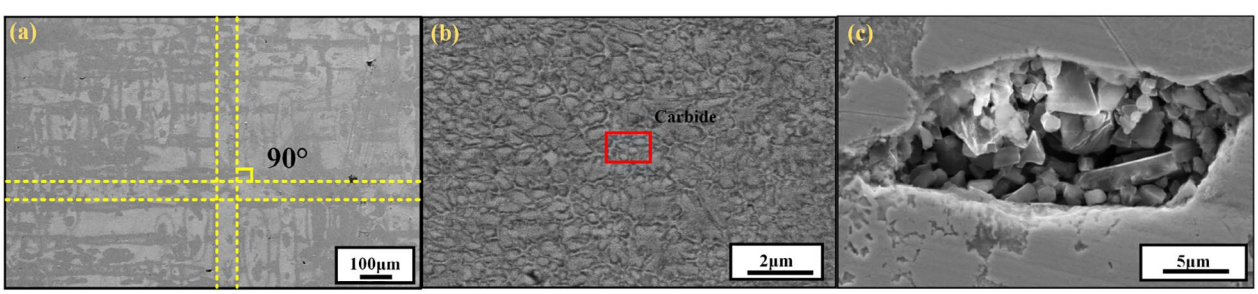

Figure 11 **a** The 90° rotation angle of each layer in SLM process, **b** Surface morphology with a network structure, **c** Micro-cracks

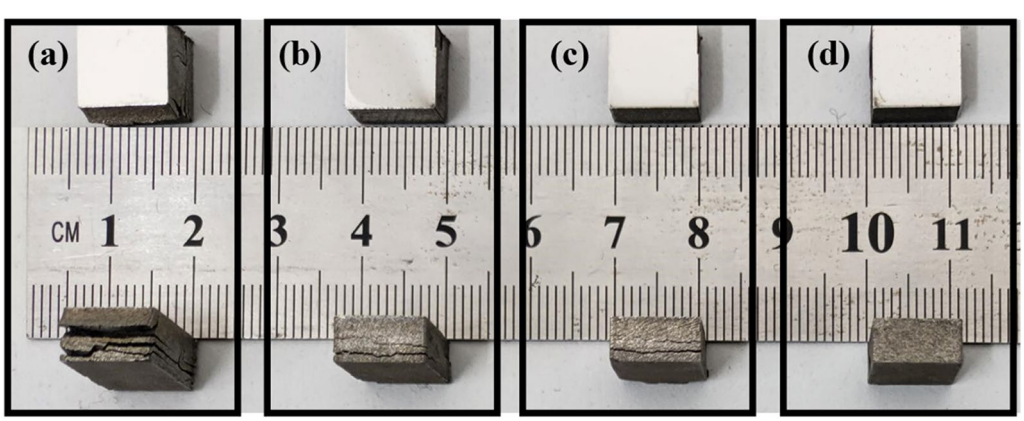

Figure 12 Side crack of cube specimens at different substrate temperatures: **a** 100 ℃, **b** 150 ℃, **c** 200 ℃, **d** 250 ℃

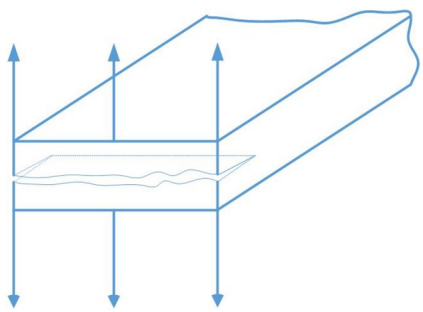

Figure 13 I opening-mode cracks in specimens

shown in Figure 12. The tensile strength increased with the gradual elimination of cracks in high substrate temperatures.

The residual stress inside the formed part is higher than the tensile strength of the material, resulting in cracks. The cracks are cold cracks with typical transgranular cracking characteristics. The rapid cooling of the molten pool during the SLM process causes a large internal residual stress inside the matrix. Under the action of residual stress, the crack propagates along the distribution of the hard brittle compound, forming I opening-mode cracks as shown in Figure 13. The residual stress can be reduced and released by optimizing the process, thereby suppressing the generation of cracks. High substrate temperature and appropriate energy density reduce the temperature gradient and inhibit crack initiation and propagation. The decrease of temperature gradient weakens the thermal expansion with the gradual increase of temperature, and the residual stress in the sample decreases. The tensile strength of SLM-formed M2 high speed steel is greatly improved by suppressing crack generation through substrate temperature.

Cracks in M2 HSS formed by SLM are mainly interlaminar cracks. The sample itself will be torn and warped due to excessive cracks since the substrate temperature is too low. The prone part is near the side of the substrate, and the cracks near the substrate become smaller, less and the Z-direction expansion range is smaller with the decrease of the temperature gradient. However, this range that only affects the crack of the molded sample near the substrate must be controlled. Because the formed layer has an impact on the unformed layer in the selective laser melting process. For example, the subsequent powder will be stuck in the powder roller, resulting in the molding cannot proceed if there is interlayer crack or even warping near the side of the substrate at the beginning of the molding. Once the laser selective melting process is stopped, that is, the printing is over, so it will produce a serious decline in the success rate of forming greatly reducing the production efficiency of parts. And the cracks generated at the beginning of printing will produce tiny cracks in the upper of the parts that affect the tensile properties because of the crack propagation. The scale characterization of interlayer cracks produced at different substrate temperatures is shown in Figure 14. The interlaminar cracks of the molded sample were more or even tearing perpendicular to the XY plane when the substrate temperature was 50 °C. The cracks near the substrate gradually decreased and the degree of cracks decreased greatly with the increase of substrate temperature. The crack size disappeared from 0.63 mm of substrate temperature at 50 °C to 0.32 mm of substrate temperature at 100 °C, 0.13 mm of substrate temperature at 150 °C, and then the macroscopic cracks disappearance at 200 °C. The substrate temperature shows the most direct impact on crack suppression.

3.3.2 Characterization of Interlaminar Cracks

In this paper, the process simulation of the molding sample is carried out to study the influence of substrate temperature on the residual thermal stress of the molding sample. The selective laser melting process involves the absorption of molding powder, the energy transfer between materials, and the characteristics of molding materials. This paper considers the energy exchange of heat conduction, heat convection and heat radiation. The differential equation is defined as :

$$k\left(\frac{\partial^2 T}{\partial x^2}+\frac{\partial^2 T}{\partial y^2}+\frac{\partial^2 T}{\partial z^2}\right)+\varepsilon\sigma\left(T^4-T_0^4\right)+h(T-T_0)=\rho c\frac{\partial T}{\partial t}, \tag{1}$$

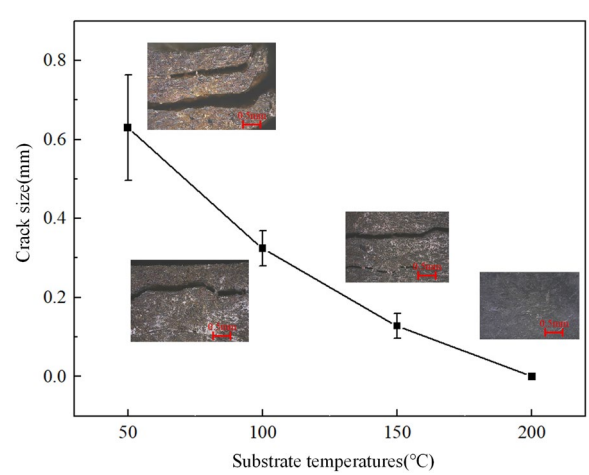

Figure 14 Crack sizes at different substrate temperatures

Table 5 Thermal physical parameters of M2 high-speed steel materials

Density(g/cm^3)	Specific heat(J/kg/K)	Thermal conductivity (W/m/K)	Emissivity	Melting point(K)	Poisson ratio μ
8.14	540	19	0.54	1793	0.26

Table 6 Process simulation molding parameters

Laser power P(W)	Scan speed v(mm/s)	Scan distance h(mm)	Layer thickness L(μm)	Substrate temperature T(℃)
220	960	0.06	0.03	50/100/150/200

where ε is the emissivity of the surface, taking 0.90; σ is Stefan-Boltzmann radiation constant of 5.67×10^{-8} W/(m^2·K^4); T is the surrounding fluid temperature, 1793 K; T_0 is the initial temperature during processing, taking 293 K; h is convective heat transfer coefficient, 12 W/(m^2·K). The impact of other factors is negligible. Mechanical deformation is calculated by:

$$\varepsilon = \varepsilon_e + \varepsilon_p + \varepsilon_{th}, \tag{2}$$

where ε_e is the elastic modulus; ε_p is plastic strain; ε_{th} is the thermal stress. The result is ε_{th} by the following equation:

$$\begin{cases} \rho\dfrac{\partial V}{\partial y} = \nabla\sigma+\rho f, \\ \sigma = f(\varepsilon), \\ \varepsilon_p=\dfrac{\partial_1^1}{\partial\sigma}, \\ \varepsilon_{th}=\alpha\Delta T, \end{cases} \tag{3}$$

$$\Delta T = \frac{D_{\text{laser}}}{V_{\text{laser}}}, \tag{4}$$

$$P_{heat} = \varphi_v Vm, \tag{5}$$

$$\varphi v = \frac{P_{\text{laser}}}{D_{\text{laser}} e_{\text{power}}}. \tag{6}$$

The thermal physical parameters of the material are shown in Table 5. Process simulation of stress field and deformation under different substrate temperatures, forming parameters are shown in Table 6. During the experiment, the maximum power of the fiber laser is 500 W, the laser spot diameter is 0.1 mm, and the laser energy distribution in the selective melting process conforms to Gaussian distribution. The laser heat source model can be expressed as:

$$q(x,y) = Q\exp\left(-2\frac{x^2+y^2}{R^2}\right), \tag{7}$$

where x and y are the coordinates relative to the laser heat source center; R is the radius of laser spot; Q is the maximum heat flux density of laser center, then:

$$Q = \frac{2\text{AP}}{\pi R^2}, \tag{8}$$

where A is the coefficient of laser energy absorbed by powder, P is laser power.

The simulation distribution of residual stress in selective laser melting M2 high-speed steel with different substrate temperatures is shown in Figure 15. M2 HSS material is formed at different substrate temperatures, the residual stress at the top of the sample is small, while the stress in the red region in the middle is large, and the residual stress is also large in the four vertical side regions of the cube. Figure 16 lists in detail the results of maximum residual stress and maximum deformation of cubic samples formed at different substrate temperatures. Different residual stresses are produced in different areas of the sample, and different degrees of deformation are caused by different cooling rates. The maximum shape variable is the smallest when the substrate temperature is 200 ℃. The maximum stress decreases with the increase of substrate temperature, and the minimum residual stress is 352 MPa when the substrate temperature is 200 ℃. Due to equipment limitations, the maximum substrate temperature is 200 ℃. In the future, the performance at higher substrate temperatures can be explored if the equipment allows.

3.3.3 Crack Formation and Suppression Mechanism

Rapid melting and solidification during SLM forming process lead to a higher cooling rate and temperature gradient in the molten pool. Cracks are mainly caused by residual stress, i.e., there is a large temperature gradient between the molten pool and solidified metal. Due to the continuous thermal cycling and complex physical/chemical reactions, the uneven heat distribution induces different amounts of the thermal expansion and cold contraction of the solidified tissue. Therefore, the SLM process is inevitably accompanied by high residual stress levels.

A large internal stress in the formed steel results in irreversible deformation. In addition, the deformation generated by the molten pool cannot be supplemented owing to the forming characteristics of SLM itself and the lack of overall liquidity, resulting in cracks. Crack formation

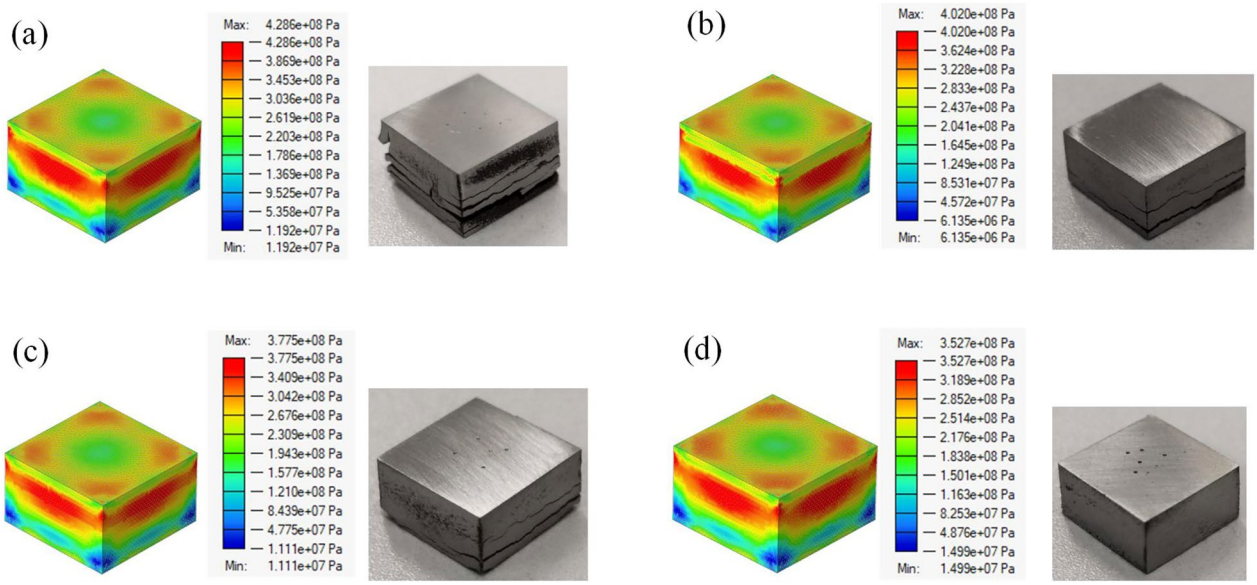

Figure 15 Simulation results of **a**–**d** substrate temperatures of 50 ℃, 100 ℃, 150 ℃ and 200 ℃, respectively

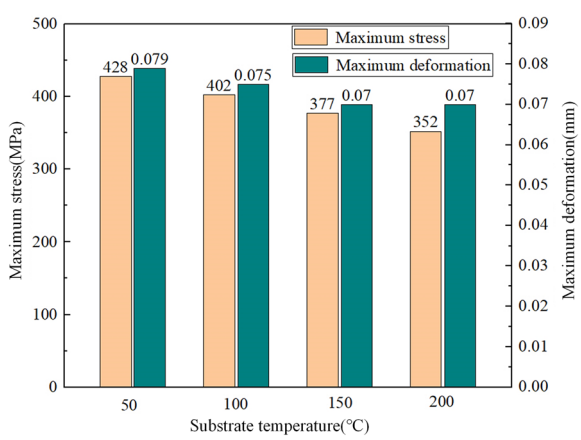

Figure 16 Simulation results of SLM forming M2 high-speed steel at different substrate temperatures

in M2 high-speed steel is even aggravated due to its high thermal conductivity, high thermal expansion coefficient and severe solidification shrinkage.

The temperature gradient mechanism results from large thermal gradients in the solid material just below the laser spot, as shown in Figure 17. Owing to the high temperature of the molded part, those upper layers will swell, while the colder underlying solidified layers will restrict this expansion. As a result, the compressive stresses σ_{comp} in the upper layers of the substrate may be higher than the yield strength of the material and cause plastic upsetting in those upper layers. The compressive stresses in the material cause plastic deformation ε_{pl} of the upper layers in case of the yield strength is reached. When those plastically upset layers cool down, their compressive state is converted into residual tensile

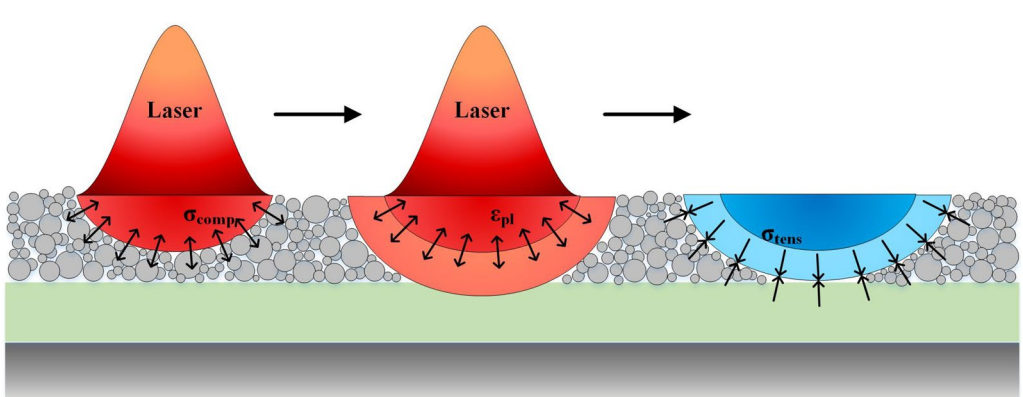

Figure 17 Temperature gradient mechanism in SLM

stresses σ_{tens}. Therefore, the compressive stress of the material due to the laser high temperature was transformed into tensile stress. When the material itself can withstand the strength that cannot be enough to offset the residual thermal stress, the parts will be deformed along the direction between the layers, resulting in interlayer cracks.

The temperature gradient is reduced and the residual stress is relatively reduced by preheating the substrate. The larger the temperature gradient, the larger the difference between the strength of the material and the residual stress, and the more obvious the crack. Considering the complexity of the SLM process and the difficulty of experimental measurement, finite element simulation methods are usually used to predict the distribution and evolution of residual stress. Residual stress of specimen exists in the form of tensile stress. The tensile stress in the sample is reduced from 428 to 352 MPa when the substrate temperature increases from 50 to 200 ℃. The substrate preheating temperature of 200 ℃ can effectively reduce the residual stress by 22% compared to 50 ℃ during processing due to the reduction of the cooling rate.

4 Conclusions

In this research, through lots of experimentation, the difficulty of laser selective melting of M2 high-speed steel is overcome, with superior mechanical properties M2 high-speed steel is fabricated, and the main results are summarized as follows.

(1) The substrate temperature has the most significant effect on mechanical properties. The optimized process parameters of laser power, scan speed, scan distance, and substrate temperature with superior mechanical properties are 220 W, 960 mm/s, 0.06 mm, and 200 ℃, respectively. Under these process parameters, the hardness and tensile strength can reach 60 HRC and 1000 MPa, respectively.

(2) The main phases of specimens are α-Fe, austenite, martensite, and MC carbides. What's more, a slight distinction in the content of M2 surface microstructure with the increase in temperature. The carbides in the sample are distributed in the network structure.

(3) Substrate temperature plays an important role in restraining the interlaminar cracks. The residual stress in the sample decreases from 428 to 352 MPa when the substrate temperature increases from 50 to 200 ℃. The cracks are suppressed due to the decrease of temperature gradient residual stress, which greatly improves the tensile strength of SLM-formed M2 high-speed steel. The results provide an experimental basis for the formation of a conformal cooling M2 high-speed steel end milling cutter using SLM.

Acknowledgements
Not applicable.

Author Contributions
WJ designed the research content and scheme. CL performed the experiment and wrote the manuscript. RD analyzed the data. SD reviewed the manuscript. All authors read and approved the final manuscript.

Authors' Information
Wenbin Ji, borned in 1985, received his PhD degree from *Shandong University*, *China* in 2017. He is currently an associate professor and master supervisor in *School of Mechanical Engineering at Hebei University of Technology, China*. He has been conducting multidisciplinary research at the crossroads of mechanics, additive manufacturing, materials science, and precision machining. Chuncheng Liu, borned in 1997, is a master candidate in *School of Mechanical Engineering, Hebei University of Technology, China*. He majors in mechanical engineering and focuses on the research of additive manufacturing of metals. Riqing Deng, borned in 1997, is a master candidate in *School of Mechanical Engineering, Hebei University of Technology, China*. He majors in mechanical engineering and focuses on the research of additive manufacturing of metals. Shijie Dai, borned in 1970, is currently a professor in *School of Mechanical Engineering, Hebei University of Technology, China*. His research interests includes intelligent robotic control and robot application.

Funding
Supported by National Natural Science Foundation of China (Grant No.52005154). Hebei Provincial Natural Science Foundation (Grant No. E2020202035).

Competing Interests
The authors declare no competing financial interests.

Received: 28 December 2021 Revised: 23 October 2022 Accepted: 16 March 2023
Published online: 05 April 2023

References

[1] N Sanaei, A Fatemi. Defects in additive manufactured metals and their effect on fatigue performance: A state-of-the-art review. *Progress in Materials Science*, 2021, 117: 100724.
[2] U Fasel, D Keidel, L Baumann, et al. Composite additive manufacturing of morphing aerospace structures. *Manufacturing Letters*, 2020, 23: 85-88.
[3] R Kumar, M Kumar, J S Chohan. The role of additive manufacturing for biomedical applications: A critical review. *Journal of Manufacturing Processes*, 2021, 64: 828-850.
[4] J Zhang, B Song, Q Wei, et al. A review of selective laser melting of aluminum alloys: Processing, microstructure, property and developing trends. *Journal of Materials Science & Technology*, 2019, 35(2): 270-284.
[5] X Zhang, Z Guo, C Chen, et al. Additive manufacturing of WC-20Co components by 3D gel-printing. *International Journal of Refractory Metals and Hard Materials*, 2018, 70: 215-223.
[6] E Uhlmann, A Bergmann, W Gridin. Investigation on additive manufacturing of tungsten carbide-cobalt by selective laser melting. *Procedia CIRP*, 2015, 35: 8-15.
[7] E Liverani, S Toschi, L Ceschini, et al. Effect of selective laser melting (SLM) process parameters on microstructure and mechanical properties of 316L austenitic stainless steel. *Journal of Materials Processing Technology*, 2017, 249: 255-263.
[8] P Kakanuru, K Pochiraju. Moisture Ingress and degradation of additively manufactured PLA, ABS and PLA/SiC composite parts. *Additive Manufacturing*, 2020, 36: 101529.

[9] K Wang, D Du, G Liu, et al. A study on the additive manufacturing of a high chromium Nickel-based superalloy by extreme high-speed laser metal deposition. *Optics & Laser Technology*, 2021, 133: 106504.
[10] A Khorasani, I Gibson, U S Awan, et al. The effect of SLM process parameters on density, hardness, tensile strength and surface quality of Ti-6Al-4V. *Additive Manufacturing*, 2019, 25: 176-186.
[11] Q B Nguyen, Z Zhu, F L Ng, et al. High mechanical strengths and ductility of stainless steel 304L fabricated using selective laser melting. *Journal of Materials Science & Technology*, 2019, 35(2): 388-394.
[12] D Sun, D Gu, K Lin, et al. Selective laser melting of titanium parts: Influence of laser process parameters on macro- and microstructures and tensile property. *Powder Technology*, 2019, 342: 371-379.
[13] W E Frazier. Metal additive manufacturing: A review. *Journal of Materials Engineering and Performance*, 2014, 23(6): 1917-1928.
[14] M Yakout, M A Elbestawi, S C Veldhuis. A study of thermal expansion coefficients and microstructure during selective laser melting of Invar 36 and stainless steel 316L. *Additive Manufacturing*, 2018, 24: 405-418.
[15] S L Sing, J An, W Y Yeong, et al. Laser and electron-beam powder-bed additive manufacturing of metallic implants: A review on processes, materials and designs. *Journal of Orthopaedic Research*, 2016, 34(3): 369-385.
[16] B Nagarajan, Z Hu, X Song, et al. Development of micro selective laser melting: the state of the art and future perspectives. *Engineering,* 2019, 5(4): 702-720.
[17] G L Zhao, L J Xin, L Li, et al. Cutting force model and damage formation mechanism in milling of 70wt% Si/Al composite. *Chinese Journal of Aeronautics*, DOI: https://doi.org/10.1016/j.cja.2022.07.018.
[18] Z H Liu, C K Chua, K F Leong, et al. Microstructural investigation of M2 high speed steel produced by selective laser melting microstructural investigation of M2 high speed steel. *Photonics & Optoelectronics, IEEE*, 2012.
[19] Z Y Liu, N H Loh, K A Khor, et al. Sintering of injection molded M2 high-speed steel. *Materials letters*, 2000, 45(1): 32-38.